Taylor & Francis
Taylor & Francis Group

Automatika

Journal for Control, Measurement, Electronics, Computing and Communications

ISSN: (Print) (Online) Journal homepage: www.tandfonline.com/journals/taut20

Analysis of the high-gain BOCUK DC-DC converter-based PFC using an LQR controller for SMPS applications

L. Annie Isabella, M.G. Umamaheswari & G. Marimuthu

To cite this article: L. Annie Isabella, M.G. Umamaheswari & G. Marimuthu (2023) Analysis of the high-gain BOCUK DC-DC converter-based PFC using an LQR controller for SMPS applications, Automatika, 64:3, 565-576, DOI: 10.1080/00051144.2023.2197823

To link to this article: https://doi.org/10.1080/00051144.2023.2197823

Published online: 16 Apr 2023.

AUTOMATIKA
2023, VOL. 64, NO. 3, 565–576
https://doi.org/10.1080/00051144.2023.2197823

REGULAR PAPER

OPEN ACCESS Check for updates

Analysis of the high-gain BOCUK DC-DC converter-based PFC using an LQR controller for SMPS applications

L. Annie Isabella[a], M.G. Umamaheswari[b] and G. Marimuthu[a]

[a]Department of Electrical and Electronics Engineering, R.M.K. Engineering College, Chennai, India; [b]Department of Electrical and Electronics Engineering, Rajalakshmi Engineering College, Chennai, India

ABSTRACT

This research work emphasizes on the development of a unique high-gain BOCUK DC-DC converter for Switched Mode Power Supply (SMPS) applications. The high-gain BOOST-CUK (BOCUK) DC-DC converter combines the benefits of both Boost and Cuk converters for attaining instantaneous line current shaping and load regulation. The proposed BOCUK converter provides a non-inverted output and improves the voltage gain and efficiency. The modes of operation of the high-gain BOCUK DC-DC Converter in a Continuous Conduction Mode (CCM) with parasitic elements in the circuit are examined and a state-space model is constructed. The second-order model is derived using the Modified Hankel Matrix Method (HMM) to make the controller design easier. Dual-loop Control employing an inner Linear Quadratic Regulator (LQR) current Controller and an outer Atom Search Optimization (ASO)-tuned Proportional Integral (PI) controller is used to analyze the performance indices of the high-gain converter and fluctuations in line, load and setpoint are investigated. Simulation results prove that the LQR controller is robust in tracking the load voltage and provides excellent line current shaping with low % Total Harmonic Distortion (THD) and nearly Unity Power Factor (UPF). The hardware model for 200W is built and implemented using the TMS320F28027F microcontroller to verify the simulation results.

ARTICLE HISTORY
Received 24 August 2022
Accepted 28 March 2023

KEYWORDS
Power factor correction (PFC); BOOST-CUK (BOCUK); linear quadratic regulator (LQR); atom search optimization (ASO); total harmonic distortion (THD)

1. Introduction

SMPS uses a switching regulator to control and stabilize the load voltage by switching the load current on and off. It has a higher power conversion efficiency and low overall power loss and hence it is a reliable power source. Smaller size, less weight, high efficiency, higher performance and flexibility are the advantages of SMPS [1–3]. High-gain DC–DC converters are a type of switching power converter that provides high-voltage gain, low switching stress, low ripple and low cost when used as SMPS. Many researchers have constructed SMPS with a two-stage conversion method [3–5] for Power Factor Correction (PFC) and load voltage control utilizing an assembly of two DC–DC converters coupled in series. Two-stage conversion is replaced here by single-stage conversion technique involving dual-loop control. The inner loop shapes the line current, and the outer loop offers load voltage regulation. Single-stage conversion technique [6–12] with dual-loop control reduces the number of components and sensors used. Discontinuous Conduction Mode (DCM)-based converters [13] are not found to be attractive since the discontinuous input inductor current distorts source current, reduces efficiency and increases losses. Isolated (Flyback, push-pull, forward, etc.) and non-isolated (buck, boost, Cuk, etc.) converters are used for power conversion in SMPS applications. A transformer makes isolated converters [13–15] undesirable as the transformer core gets saturated. Due to the lack of a transformer, non-isolated converter topologies are typically preferred over isolated converter topologies and it has the following advantages such as low cost, small size, minimal weight, reduced losses and high efficiency. PFC converters play a vital role in reducing the high harmonic current levels and poor power factors in SMPS applications. PFC converters permit effective line current shaping and regulated load voltage. Protection of the utility from peak currents and emulation of the converter circuit as a resistor are desirable for implementing DC–DC converters in several applications. The Boost, Cuk and SEPIC converters prove more effective among DC–DC converters in PFC due to an input side inductance which is in series with the bridge rectifier. Boost converters [16] are often used for PFC,

CONTACT L. Annie Isabella annieisabella360@gmail.com Department of Electrical and Electronics Engineering, R.M.K. Engineering College, Tamil Nadu, India

but they have significant drawbacks, including limited voltage gain, high-voltage stress over the semiconductor switch and high reverse recovery current across the diode, all of which reduce the converter's efficiency. The DC–DC Cuk converter [17,18] can provide the load voltage with polarity inversion. This converter also offers good isolation, variation in voltage magnitude, current limit, higher steady-state performance and protection towards the short circuit. High current stresses on the switch and diode are major drawbacks of the DC–DC Cuk converter.

The BOCUK Converter with a single power semiconductor switch has the benefits such as an increase in voltage gain and a reduction in voltage stress between the power switch and diodes [19] when compared to the conventional boost architecture. The input and output currents are both continuous in the derived BOCUK topology, resulting in a non-inverted output. Nonideal elements, such as an equivalent series resistor (ESR), the voltage drop on-state resistance and forward voltage drop (FVD), exist in inductors, capacitors and semiconductor devices. Nonideal effects become more noticeable as diode forward voltage drops vary between 0.3 V and 1 V. To address these issues, the LQR based nonideal high-gain BOCUK Converter is proposed in this research work.

Optimization-based metaheuristic algorithms have been currently employed by many researchers for power electronic applications. Meta-heuristics iteratively improve an initial solution created by some heuristic until a stopping requirement is reached. Genetic Algorithm (GA) [12], Particle Swarm Optimization (PSO) [20], Grey Wolf Optimizer (GWO) [21], etc. are some of the metaheuristic algorithms that have recently been used. Atom Search Optimization (ASO) is utilized here since it offers accurate, consistent, effective and efficient optimization for tuning the outer PI controller parameters leading to regulated load voltage.

The LQR control [22–24] is a well-known method for optimizing the cost function. In this control scheme, the researcher can choose the proper weighing matrices based on which state variables are more significant in the control action to obtain optimal performance. A time-varying LQR is used to shape the line current so that it is in phase with the line voltage. LQR generates an infinite gain margin demonstrating its robustness and is computationally efficient. The state-space model of the non-ideal BOCUK converter is derived and from the fifth-order model, the Hankel matrix technique is utilized to construct the second-order model. The simplified second-order model is employed for the easy design of LQR controller feedback gains and PI controller parameters. The major goal of this research is to derive the mathematical model of the BOCUK and to design the optimally stable controller with the ASO algorithm-tuned PI and LQR controller. The proposed BOCUK is then imperilled to closed-loop control using outer ASO-tuned PI and inner LQR to eliminate input current harmonics and improve performance characteristics such as nearly UPF, low % THD, low % regulation and less settling time for line, load and setpoint fluctuations.

2. Modes of operation, state-space model & design of components of the BOCUK converter

This section discusses the modelling, its components design and the determination of the second-order model of the BOCUK Converter. Figure 1 demonstrates the circuit of the BOCUK Converter and the waveform illustrating its modes of operation are also presented in Figure 2(c). The state-space model is derived from the dynamics of converter components during Sub-interval I and Sub-interval II.

The BOCUK converter including the parasitic elements operates in two modes with S On and Diodes in the Off state and S Off and Diodes in the On state in Continuous conduction mode. During the transition of state to the next mode of operation, diode D_2 starts conducting initially and it conducts only for a small period of (1–k). Since it conducts for less duration, this case is not considered. The state-space equations are derived considering the current through the inductors i_{L1} and

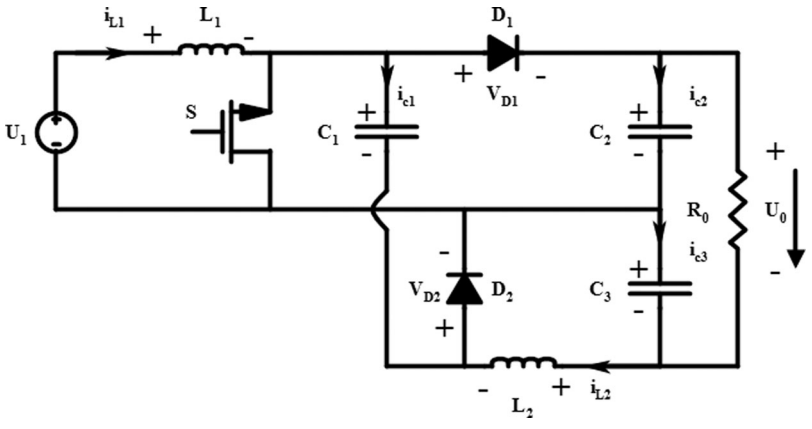

Figure 1. The BOCUK converter.

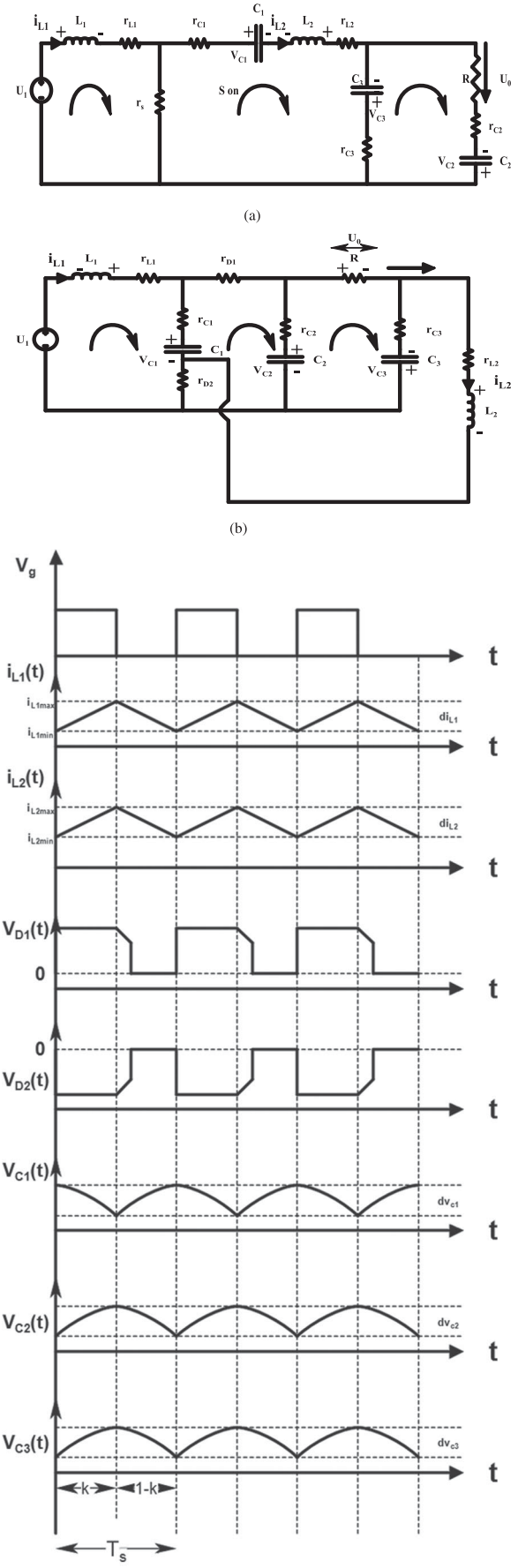

Figure 2. (a) Sub-interval I: S On, D1 Off, D2 Off; (b) Sub-interval II: S Off, D1 On, D2 On; (c) Theoretical waveforms of the BOCUK converter.

i_{L2} and the voltage across the transfer capacitor v_{C1} and output capacitors v_{C2} and v_{C3} as the state variables. Employing KVL and KCL for the equivalent circuit of each mode, the state-space equations are developed.

2.1. Sub-interval I

The circuit of this Sub-interval I is shown in Figure 2(a). The Switch is turned On and both the diodes D_1 and D_2 are turned Off. Inductors L_1 and L_2 charge and Capacitor C_1 discharges through inductor L_2 and the switch. The diodes D_1 and D_2 are kept in the OFF state by the blocking voltage of Capacitors C_1 and C_2. The KVL and KCL equations are employed to obtain the state-space equations. The parameters A_1 B_1 C_1 D_1 are given by the following equations.

$$\dot{x}_1 = \frac{V_s}{L_1} - \frac{x_1}{L_1}(r_{L1} + r_s) + \frac{r_s x_2}{L_1} \tag{1}$$

$$\dot{x}_2 = \frac{r_s x_1}{L_2} - \frac{x_2}{L_2}(r_s + r_{L2}) - \frac{x_3}{L_2} + x_5 \tag{2}$$

$$\dot{x}_3 = \frac{x_2}{C_1} \tag{3}$$

$$\dot{x}_4 = \frac{-x_4}{RC_2} - \frac{x_5}{RC_2} \tag{4}$$

$$\dot{x}_5 = -\frac{x_2}{RC_3} - \frac{x_4}{RC_3} - \frac{x_5}{RC_3} \tag{5}$$

$$x(t) = \begin{bmatrix} i_{L1} & i_{L2} & v_{C1} & v_{C2} & v_{C3} \end{bmatrix}^T \tag{6}$$

$$y(t) = \begin{bmatrix} i_{L1} & v \end{bmatrix}^T \tag{7}$$

$$u(t) = \begin{bmatrix} v_{in} & V_{D1} & V_{D2} \end{bmatrix}^T \tag{8}$$

$$A_1 = \begin{bmatrix} -\frac{(r_{L1}+r_s)}{L_1} & \frac{r_s}{L_1} & 0 & 0 & 0 \\ \frac{r_s}{L_2} & -\frac{(r_s+r_{L2})}{L_2} & -\frac{1}{L_2} & 0 & 1 \\ 0 & \frac{1}{C_1} & 0 & 0 & 0 \\ 0 & 0 & 0 & -\frac{1}{RC_2} & -\frac{1}{RC_2} \\ 0 & -\frac{1}{RC_3} & 0 & -\frac{1}{RC_3} & -\frac{1}{RC_3} \end{bmatrix} \tag{9}$$

$$B_1 = \begin{bmatrix} \frac{1}{L_1} & 0 & 0 & 0 & 0 \\ 0 & 0 & 0 & 0 & 0 \\ 0 & 0 & 0 & 0 & 0 \end{bmatrix}^T \tag{10}$$

$$C_1 = \begin{bmatrix} 1 & 0 & 0 & 0 & 0 \\ 0 & 0 & 0 & 1 & 1 \end{bmatrix} \tag{11}$$

$$D_1 = [0] \tag{12}$$

Substituting the values of internal resistances, inductance and capacitances, the matrices A_1, B_1, C_1 and D_1 are as follows:

$$A_1 = \begin{bmatrix} -2.9 & 1.9 & 0 & 0 & 0 \\ 3.8 & -5.8 & -2000 & 0 & 1 \\ 0 & 100000 & 0 & 0 & 0 \\ 0 & 0 & 0 & -10 & -10 \\ 0 & -10 & 0 & -10 & -10 \end{bmatrix} \tag{13}$$

$$B_1 = \begin{bmatrix} 1000 & 0 & 0 & 0 & 0 \\ 0 & 0 & 0 & 0 & 0 \\ 0 & 0 & 0 & 0 & 0 \end{bmatrix}^T \quad (14)$$

$$C_1 = \begin{bmatrix} 1 & 0 & 0 & 0 & 0 \\ 0 & 0 & 0 & 1 & 1 \end{bmatrix} \quad (15)$$

$$D_1 = [0] \quad (16)$$

2.2. Sub-interval II

The circuit of this Sub-interval II is shown in Figure 2(b). The Switch is turned Off and both the diodes D_1 and D_2 are turned On. The inductors L_1 and L_2 discharge which turns On diode D_1 and the Capacitors C_1 and C_2 charge through L_1 to turn On diode D_2 to deliver the load current. The KVL and KCL equations are employed to obtain the state-space equations. The matrices A_2, B_2, C_2 and D_2 are given by the following equations.

$$\dot{x}_1 = \frac{V_s}{L_1} - \frac{r_{L1}}{L_1}x_1 - \frac{1}{L_1}x_4 - V_{D1} \quad (17)$$

$$\dot{x}_2 = -\frac{r_{L2}}{L_2}x_2 + x_5 + V_{D2} \quad (18)$$

$$\dot{x}_3 = \frac{x_1}{C_1 + C_2} - \frac{x_3}{R(C_1 + C_2)} - \frac{x_4}{R(C_1 + C_2)} \quad (19)$$

$$\dot{x}_4 = \frac{x_1}{C_1 + C_2} - \frac{x_3}{R(C_1 + C_2)} - \frac{x_4}{R(C_1 + C_2)} \quad (20)$$

$$\dot{x}_5 = \frac{-x_2}{C_3} - \frac{x_4}{RC_3} - \frac{x_5}{RC_3} \quad (21)$$

$$A_2 = \begin{bmatrix} -\frac{r_{L1}}{L_1} & 0 & 0 & -\frac{1}{L_1} & 0 \\ 0 & -\frac{r_{L2}}{L_2} & 0 & 0 & 1 \\ \frac{1}{C_1+C_2} & 0 & -\frac{1}{R(C_1+C_2)} & -\frac{1}{R(C_1+C_2)} & 0 \\ \frac{1}{C_1+C_2} & 0 & -\frac{1}{R(C_1+C_2)} & -\frac{1}{R(C_1+C_2)} & 0 \\ 0 & \frac{-1}{C_3} & 0 & -\frac{1}{RC_3} & -\frac{1}{RC_3} \end{bmatrix} \quad (22)$$

$$B_2 = \begin{bmatrix} \frac{1}{L_1} & 0 & 0 & 0 & 0 \\ -1 & 0 & 0 & 0 & 0 \\ 0 & 1 & 0 & 0 & 0 \end{bmatrix}^T \quad (23)$$

$$C_2 = \begin{bmatrix} 1 & 0 & 0 & 0 & 0 \\ 0 & 0 & 0 & 1 & 1 \end{bmatrix} \quad (24)$$

$$D_2 = [0] \quad (25)$$

Substituting the values of internal resistances, inductance and capacitances, the matrices A_2, B_2, C_2 and D_2 are as follows:

$$A_2 = \begin{bmatrix} -1 & 0 & 0 & -1000 & 0 \\ 0 & -2 & 0 & 0 & 1 \\ 497.5 & 0 & -9.95 & -9.95 & 0 \\ 497.5 & 0 & -9.95 & -9.95 & 0 \\ 0 & -500 & 0 & -10 & -10 \end{bmatrix} \quad (26)$$

$$B_2 = \begin{bmatrix} 1000 & 0 & 0 & 0 & 0 \\ -1 & 0 & 0 & 0 & 0 \\ 0 & 1 & 0 & 0 & 0 \end{bmatrix}^T \quad (27)$$

$$C_2 = \begin{bmatrix} 1 & 0 & 0 & 0 & 0 \\ 0 & 0 & 0 & 1 & 1 \end{bmatrix} \quad (28)$$

$$D_2 = [0] \quad (29)$$

From the KVL and KCL equations obtained in Sub-interval I and Sub-interval II, the following expressions are rewritten to derive the transfer function. Using the related expressions, the converter components are found .

$$V_s = L_1\frac{\Delta I_1}{t_1} \quad (30)$$

$$V_s - V_{c_1} = L_1\frac{\Delta I_1}{t_2} \quad (31)$$

$$L_1\frac{\Delta I_2}{t_1} = V_o + 2V_{c_1} \quad (32)$$

$$L_2\frac{\Delta I_2}{t_2} = V_o - V_{c_1} \quad (33)$$

$$\Delta I_1 = \frac{V_s t_1}{L_1} = \frac{(V_s V_{c1})t_2}{L_1} \quad (34)$$

$$\Delta I_2 = \frac{(V_{o+}2Vc_1)t_1}{L_2} = \frac{(V_{o-}Vc_1)t_2}{L_2} \quad (35)$$

From Equation (34), V_{c_1} is written as

$$V_{c_1} = \frac{V_s(1-2k)}{(1-k)} \quad (36)$$

From Equation (35), V_{c_1} is written as

$$V_{c_1} = \frac{V_o(1-2k)}{(1+k)} \quad (37)$$

From Equation (36) and (37), $\frac{V_o}{V_s} = \frac{1+k}{1-k}$ (37 a)

From Equation (30)

$$L_1 = V_s\frac{t_1}{\Delta i_{L1}}$$

$$L_1 = V_s\frac{kT}{\Delta i_{L1}}$$

$$L_1 = V_s\frac{k}{f_s\Delta i_{L1}} \quad (38)$$

$$L_2 = \frac{L_1}{2} \quad (39)$$

$$C_1 = \frac{\Delta Q}{\Delta V_{c1}} = \frac{\mathrm{T}\,\Delta I_{L2}}{8\,\Delta V_{c1}} = \frac{\Delta I_{L2}}{8\mathrm{f}\,\Delta V_{c1}} \quad (40)$$

$$i_c(t) = C_2\frac{\mathrm{d}V_c(t)}{dt}$$

$$i_c(t) = C_2\frac{\Delta V_c(t)}{\Delta t}$$

$$C_2 = \frac{i_c(\mathrm{t})\Delta t}{\Delta V c_2} = \frac{I_o\,\mathrm{k}T}{\Delta V c_2} = \frac{I_o\,\mathrm{k}}{f\Delta V c_2} \quad (41)$$

Table 1. Parasitic components of the BOCUK converter.

Component	L_1	L_2	C_1	C_2	C_3	S	D_1	D_2
Symbol	r_{L1}	r_{L2}	r_{C1}	r_{C2}	r_{C3}	r_S	r_{D1}	r_{D2}
Value Ω	$1e^{-3}$	$1e^{-3}$	$10e^{-6}$	$20e^{-6}$	$20e^{-6}$	$1.9e^{-3}$	$1e^{-3}$	$1e^{-3}$

$$C_3 = \frac{i_c(\mathrm{t})\Delta t}{\Delta V c_3} = \frac{I_o\,\mathrm{k}T}{\Delta V c_3} = \frac{I_o\,\mathrm{k}}{f\Delta V c_3} \tag{42}$$

Theoretical waveforms for the Sub-intervals I and II are represented in Figure 2(c). The BOCUK Converter operating in CCM is designed with various parameters provided by the specifications: Line Voltage $V_s = 24$ V, Load/Output Voltage $V_o = 100$ V, Load Resistance $R = 50\,\Omega$, switching frequency $f_s = 50$ KHz, Load Current $I_o = (0–2)$ A, Duty ratio $k = 0.62$, Ripple in the inductor current = 0.14 A, Capacitor voltage ripple $\Delta V_c = (0–1)$ V. Table 1 depicts the values of the parasitic components. For continuous conduction, after substituting all the chosen value inductor and capacitor values for the input and output sides are calculated as follows.

$$L_1 = \frac{V_s k}{f_s \Delta i_{L1}} = \frac{24 * 0.6219}{100 * 10^3 * 0.14} = 1mH \tag{43}$$

$$\mathrm{L}_2 = \frac{\mathrm{L}_1}{2} = 0.5mH \tag{44}$$

$$\mathrm{C}_1 = \frac{\Delta \mathrm{I}_2}{8\mathrm{f}\Delta \mathrm{Vc}_1} = \frac{0.0745}{8*100*10^3*0.009} = 10\mu\mathrm{F} \tag{45}$$

$$\mathrm{C}_2 = \frac{\mathrm{I}_o\,\mathrm{k}}{\mathrm{f}\Delta \mathrm{Vc}_2} = \frac{2*0.6219}{100*10^3*0.06} = 2000\mu\mathrm{F} \tag{46}$$

$$\mathrm{C}_3 = \frac{\mathrm{I}_o\,\mathrm{k}}{\mathrm{f}\Delta \mathrm{Vc}_2} = \frac{2*0.6219}{100*10^3*0.06} = 2000\mu\mathrm{F} \tag{47}$$

2.3. Derivation of second-order model using HMM

The converter dynamics is modelled using the state-space averaging technique and the state-space model of the converter operating in equilibrium is obtained after perturbation of the duty cycle. The control to input transfer function (G_{id}) and control to output transfer function (G_{vd}) are acquired by the following equations.

$$\begin{cases} \frac{d\hat{x}(t)}{dt} = A\hat{x}(t) + \{(A_1 - A_2)X + (B_1 - B_2)U\}\hat{d}(t) \\ \hat{y}(t) = C\hat{x}(t) + \{(C_1 - C_2)X\}\hat{d}(t) \end{cases} \tag{48}$$

$\hat{\boldsymbol{x}}(t), \hat{\boldsymbol{u}}(t), \hat{\boldsymbol{y}}(t)$ denote the perturbed value of the state, input and output vectors, respectively. The quantities X, U and D denote the equilibrium (DC) state, input vectors and duty cycle, respectively. The averaged state matrix A, input matrix B and output matrix C are given by

$$A = DA_1 + (1 - D)A_2 \tag{49}$$

$$B = DB_1 + (1 - D)B_2 \tag{50}$$

$$C = DC_1 + (1 - D)C_2 \tag{51}$$

The expression to find the transfer function of BOCUK Converter from the state equations is given by

$$\begin{bmatrix} G_{id}(s) \\ G_{vd}(s) \end{bmatrix} = C(sI - A)^{-1}\{(A_1 - A_2)X + (B_1 - B_2)U\} + (C_1 - C_2)X \tag{52}$$

The corresponding fifth-order transfer functions obtained are given below:

$$G_{id}(s) = \frac{2.399e^4s^4 + 9.55e^7s^3 + 2.978e^{12}s^2 + 5.94e^{13}s - 7.094e^{11}}{s^5 + 26.55s^4 + 7.6958e^7s^3 + 1.76e^9s^2 - 4.4724e^9s - 4.46e^{10}} \tag{53}$$

$$G_{vd}(s) = \frac{1502s^4 + 1.03e^7s^3 + 9.636e^{10}s^2 + 5.639e^{14}s - 8.994e^{12}}{s^5 + 26.55s^4 + 7.6958e^7s^3 + 1.76e^9s^2 - 4.4724e^9s - 4.46e^{10}} \tag{54}$$

The transfer function of the BOCUK converter is of fifth-order and hence the design of the inner LQR and ASO-tuned outer PI controller entails more computation time. Here Type -I HMM is utilized to get the second-order reduced order model of the inner current PI loop. G_{id} (s) is reduced to second-order model without losing the real converter performance. Similarly, to tune the ASO-based outer PI loop, the transfer function $G_{vi}(s) = G_{vd}(s)/G_{id}(s)$ must be reduced to the second order. The original G_{vi} transfer function is of order nine. The Hankel matrix for the fifth-order system is represented by the given equation $H_{ij}{}^{(0)}$ with i = j = 5

$$H_{55}{}^{(0)} = \begin{bmatrix} CA^{-1}B & CB & CAB & CA^2B & CA^3B \\ CB & CAB & CA^2B & CA^3B & CA^4B \\ CAB & CA^2B & CA^3B & CA^4B & CA^5B \\ CA^2B & CA^3B & CA^4B & CA^5B & CA^6B \\ CA^3B & CA^4B & CA^5B & CA^6B & CA^7B \end{bmatrix} = X * Y \tag{55}$$

X = controllability and Y = observability

$$H_{55}{}^{(0)} = \begin{bmatrix} e_{11} & e_{12} & e_{13} & e_{14} & e_{15} \\ e_{21} & e_{22} & e_{23} & e_{24} & e_{25} \\ e_{31} & e_{32} & e_{33} & e_{34} & e_{35} \\ e_{41} & e_{42} & e_{43} & e_{44} & e_{45} \\ e_{51} & e_{52} & e_{53} & e_{54} & e_{55} \end{bmatrix} \tag{56}$$

$$H_{55}{}^{(1)} = H_{55}{}^{(0)} - \frac{1}{e_{11}} \begin{bmatrix} z \\ e_{21} \\ e_{31} \\ e_{41} \\ e_{51} \end{bmatrix}$$

$$\times \begin{bmatrix} e_{11} & e_{12} & e_{13} & e_{14} & e_{15} \end{bmatrix} \quad (57)$$

where $z = e_{11}$-1

$$H_{55}{}^{(1)} = \begin{bmatrix} 1 & e_{12}{}' & e_{13}{}' & e_{14}{}' & e_{15}{}' \\ 0 & e_{22}{}' & e_{23}{}' & e_{24}{}' & e_{25}{}' \\ 0 & e_{32}{}' & e_{33}{}' & e_{34}{}' & e_{35}{}' \\ 0 & e_{42}{}' & e_{43}{}' & e_{44}{}' & e_{45}{}' \\ 0 & e_{52}{}' & e_{53}{}' & e_{54}{}' & e_{55}{}' \end{bmatrix} \quad (58)$$

$$H_{55}{}^{(2)} = \begin{bmatrix} 1 & 0 & e_{13}{}'' & e_{14}{}'' & e_{15}{}'' \\ 0 & 1 & e_{23}{}'' & e_{24}{}'' & e_{25}{}'' \\ 0 & 0 & e_{33}{}'' & e_{34}{}'' & e_{35}{}'' \\ 0 & 0 & e_{43}{}'' & e_{44}{}'' & e_{45}{}'' \\ 0 & 0 & e_{53}{}'' & e_{54}{}'' & e_{55}{}'' \end{bmatrix} \quad (59)$$

$$H_{55}{}^{(3)} = \begin{bmatrix} 1 & 0 & 0 & e_{14}{}''' & e_{15}{}''' \\ 0 & 1 & 0 & e_{24}{}''' & e_{25}{}''' \\ 0 & 0 & 1 & e_{34}{}''' & e_{35}{}''' \\ 0 & 0 & 0 & e_{44}{}''' & e_{45}{}''' \\ 0 & 0 & 0 & e_{54}{}''' & e_{55}{}''' \end{bmatrix} \quad (60)$$

The second-order reduced model is now obtained

$$A_2{}^{-1} = \begin{bmatrix} 0 & e_{13}{}''' \\ 1 & e_{23}{}''' \end{bmatrix} \quad (61)$$

$$B_2 = \begin{bmatrix} 1 \\ 0 \end{bmatrix} \quad (62)$$

$$\mathrm{C}_2 = \begin{bmatrix} \mathrm{e}_{11} & \mathrm{e}_{12} \end{bmatrix} \quad (63)$$

The reduced order state matrices for the inner current PI loop are given by

$$A_2 = \begin{bmatrix} 0 & 17.95 \\ 1 & -2.71 \end{bmatrix} \quad (64)$$

$$\mathrm{B}_2 = \begin{bmatrix} 1 \\ 0 \end{bmatrix} \quad (65)$$

$$\mathrm{C}_2 = \begin{bmatrix} 2.3\mathrm{e}4 & -286.4 \end{bmatrix} \quad (66)$$

The second-order reduced order transfer function $G_{id}(s)$ of the BOCUK Converter is given by

$$G_{id}(s) = \frac{2.399e^4 s - 286.4}{s^2 + 2.71s - 17.95} \quad (67)$$

The ninth-order transfer function to tune the outer voltage PI loop is given by the following equation :

$$\mathrm{G_{vi}}(\mathrm{s}) = \frac{\begin{array}{c} 1502\mathrm{s}^4 + 1.03\mathrm{e}^7\mathrm{s}^8 + 2.122\mathrm{e}^{11}\mathrm{s}^7 \\ +1.36\mathrm{e}^{15}\mathrm{s}^6 - 7.488\mathrm{e}^{18}\mathrm{s}^5 + 4.356\mathrm{e}^{22}\mathrm{s}^4 \\ +9.924\mathrm{e}^{23}\mathrm{s}^3 + 2.501\mathrm{e}^{24}\mathrm{s}^2 - 2.511\mathrm{e}^{25}\mathrm{s} \\ +3.998\mathrm{e}^{23} \end{array}}{\begin{array}{c} 2.399\mathrm{e}^4\mathrm{s}^9 + 9.617\mathrm{e}^7\mathrm{s}^8 + 4.826\mathrm{e}^{12}\mathrm{s}^7 \\ +7.582\mathrm{e}^{15}\mathrm{s}^6 + 2.293\mathrm{e}^{20}\mathrm{s}^5 + 9.813\mathrm{e}^{21}\mathrm{s}^4 \\ +1.178\mathrm{e}^{23}\mathrm{s}^3 + 1.32\mathrm{e}^{23}\mathrm{s}^2 - 2.644\mathrm{e}^{24}\mathrm{s} \\ +3.154\mathrm{e}^{22} \end{array}} \quad (68)$$

The reduced order state matrices for the outer voltage PI loop are

$$A_2 = \begin{bmatrix} 0 & -0.2265 \\ 1 & -19.06 \end{bmatrix} \quad (69)$$

$$B_2 = \begin{bmatrix} 1 \\ 0 \end{bmatrix} \quad (70)$$

$$C_2 = \begin{bmatrix} 180 & 2.857 \end{bmatrix} \quad (71)$$

The second-order reduced order transfer function $G_{vi}(s)$ of the BOCUK Converter is given by

$$G_{vi}(s) = \frac{180s + 2.857}{s^2 + 19.06s + 0.2265} \quad (72)$$

3. Closed-loop control of the BOCUK converter

Figure 3 illustrates the dual-loop control of the BOCUK converter, with the ASO-based PI Controller acting as the outer voltage loop and LQR acting as the inner current controller. The BOCUK DC-DC Converter's load voltage is measured and compared to a reference voltage of 100 V, with the voltage error (e_v) being fed into the ASO-based PI controller as an input. By multiplying the absolute value of input voltage with the ASO-tuned PI controller output, the current reference for the inner loop is generated. The inner LQR controller uses the control law $u = -G_x$ to force the input inductor current to follow the current reference set by the ASO-tuned PI controller. The voltage error (e_v), current error (e_i) and feedback gains G_1 and G_2 are used to generate the control law. The BOCUK converter's switch is triggered by the resultant switching pulse, which offers UPF operation and regulated load voltage. Derivations of gains G_1 and G_2 (0.5 and 350) are discussed in section 4.2.

3.1. Design of the ASO-optimized outer PI voltage controller

To increase the dynamic performance of the BOCUK converter, the ASO algorithm is utilized to determine the appropriate PI controller parameter values. The optimization process begins with ASO generating a set of random solutions. Each iteration updates the positions and velocities of the atoms, as well as the position of the best atom is discovered. Furthermore, the acceleration of atoms is caused by two factors. The Lennard-Jones potential, which is the vector sum of the attraction and repulsion exerted by other atoms, is one source of interaction force (F_i). The bond-length potential, which is the weighted position difference between each atom and the best atom, is another constraint force (H_i). All the updates and calculations are done in real-time until the stopping requirement is met. As global optimal values, the position and fitness values of the best atom are returned. The algorithmic steps implemented for the tuning of the PI controller are listed below:

Step 1: Initialize the K_P and K_I values of the PI controller using the Ziegler-Nicholas method.

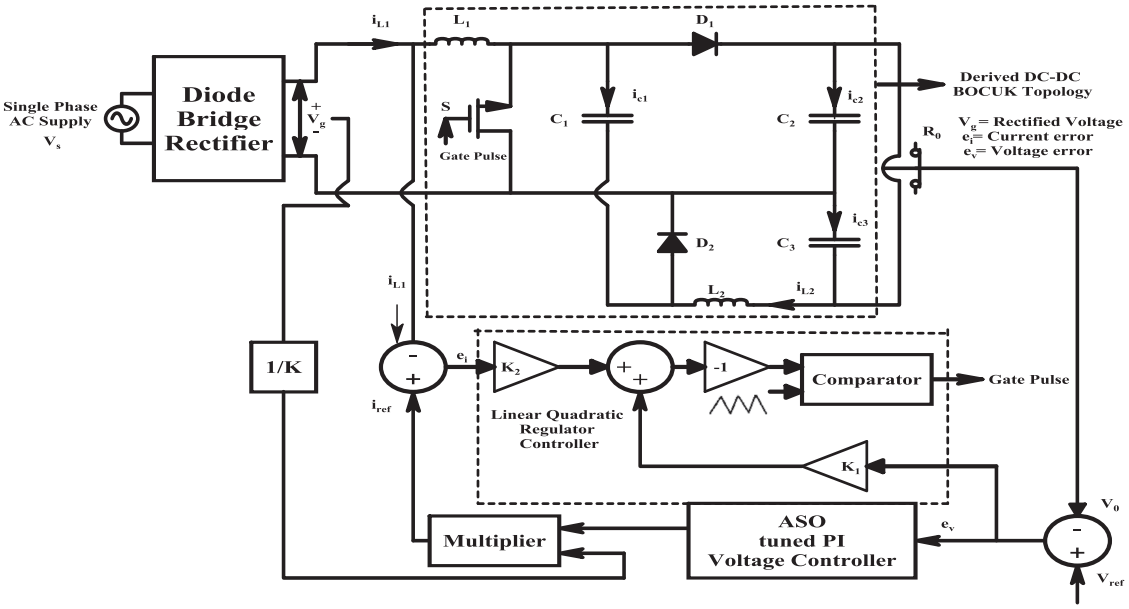

Figure 3. Closed-loop control of the BOCUK converter.

Step 2: Define population size, cost function, boundary condition and constant parameters. Initialize positions x, velocities v of atoms and the number of iterations.

Step 3: Simulate the initial value of K_P and K_I.

Step 4: Calculate the error using Integral Square Error (ISE) fitness Criterion. If the fitness value is minimum, select the fittest value according to the fitness function.

Step 5: Compute atom mass, define its K Neighbours, and Compute Fi, Gi and acceleration.

Step 6: Update the velocities and positions and increase the iteration by one.

Step 7: If the maximum number of iterations is satisfied, find the optimal parameters of K_P and K_I [0.97,9.7]. Else continue from step 2.

3.2. Design of the inner LQR current controller

The LQR approach is a powerful strategy that aims to identify the best controller that minimizes a given cost function. Weighing matrices Q, R, system equivalent input ($u_e(t)$) and error ($e(t)$) are used to define the cost function. The LQR technique is based on the state-space model and aims to find the appropriate control law by solving the Riccati equation algebraically. The dynamic system is expressed as

$$\begin{bmatrix}\dot{x}(t)\\ \dot{\varepsilon}(t)\end{bmatrix}=\begin{bmatrix}A & 0\\ -C & 0\end{bmatrix}\begin{bmatrix}x\\ \varepsilon\end{bmatrix}+\begin{bmatrix}B\\ 0\end{bmatrix}\mu+\begin{bmatrix}0\\ I\end{bmatrix}\gamma \quad (73)$$

$x(\alpha)$, $\varepsilon(\alpha)$ & $\mu(\alpha)$ approach constant value, then $\varepsilon = 0$, so $y(\alpha) = \gamma$.

Here x = state vector, u = control signal, y = output, γ = reference (step function/scalar) and ε = the output of integrator.

In steady state

$$\begin{bmatrix}\dot{x}(\alpha)\\ \dot{\varepsilon}(\alpha)\end{bmatrix}=\begin{bmatrix}A & 0\\ -C & 0\end{bmatrix}\begin{bmatrix}\dot{x}(\alpha)\\ \dot{\varepsilon}(\alpha)\end{bmatrix}+\begin{bmatrix}B\\ 0\end{bmatrix}\mu(\alpha)+\begin{bmatrix}0\\ I\end{bmatrix}\gamma(\alpha) \quad (74)$$

$r(t)\rightarrow$ signed step then,

$r(\alpha) = \gamma(t) = \gamma$ is a constant value, $t > 0$

Using Equations (73) & (74)

$$\begin{bmatrix}\dot{x}(t)- & \dot{x}(\alpha)\\ \dot{\varepsilon}(t)- & \dot{\varepsilon}(\alpha)\end{bmatrix}=\begin{bmatrix}A & 0\\ -C & 0\end{bmatrix}\begin{bmatrix}x(t)- & x(\alpha)\\ \varepsilon(t)- & \varepsilon(\alpha)\end{bmatrix}+\begin{bmatrix}B\\ 0\end{bmatrix}[u(t)-u(\alpha)] \quad (75)$$

$$\begin{bmatrix}\dot{x}_e(t)\\ \dot{\varepsilon}_e(\alpha)\end{bmatrix}=\begin{bmatrix}A & 0\\ -C & 0\end{bmatrix}\begin{bmatrix}x_e(t)\\ \varepsilon_e(t)\end{bmatrix}+\begin{bmatrix}B\\ 0\end{bmatrix}u_e(t) \quad (76)$$

With

$$u_e(t) = -Gx_e(t) + G_I\varepsilon_e(t) \quad (77)$$

$$e(t)=\begin{bmatrix}x_e(t)\\ \varepsilon_e(t)\end{bmatrix} \quad (78)$$

$$\dot{e} = \hat{A}e + \hat{B}u_e \quad (79)$$

$$\hat{A}=\begin{bmatrix}A & 0\\ -C & 0\end{bmatrix}, \hat{B}=\begin{bmatrix}B\\ 0\end{bmatrix} \quad (80)$$

$$\hat{A}=\begin{bmatrix}0.2275 & 0\\ -180 & 0\end{bmatrix}, \hat{B}=\begin{bmatrix}1\\ 0\end{bmatrix} \quad (81)$$

$$u_e = -Ge, \hat{G} = (G - G_I) \quad (82)$$

$$\dot{e} = (\hat{A} - \hat{B}\hat{G})e \quad (83)$$

Value is found $\hat{G}$ using the LQR methodology, and the cost function is given as

$$J = \tfrac{1}{2}\int_0^{\alpha}(e^T Q_e + u_e^T R u_e)dt \quad (84)$$

& Riccati equation,

$$\hat{A}^T\hat{G} + \hat{G}\hat{A} + \hat{Q} - \hat{G}\hat{B}R^{-1}B^T\hat{G} = 0 \qquad (85)$$

On solving the Riccati equation, the values of G_1 and G_2 are 0.5 and 350, respectively. Implementing it in the control law provides UPF operation and regulated load voltage.

4. Simulation results

Simulation is done using MATLAB/SIMULINK R2014a to assess system performance. A simulation model of a non-ideal BOCUK PFC Converter controlled by the dual-loop control scheme is constructed. Figure 4(a) depicts the simulated line current and line voltage

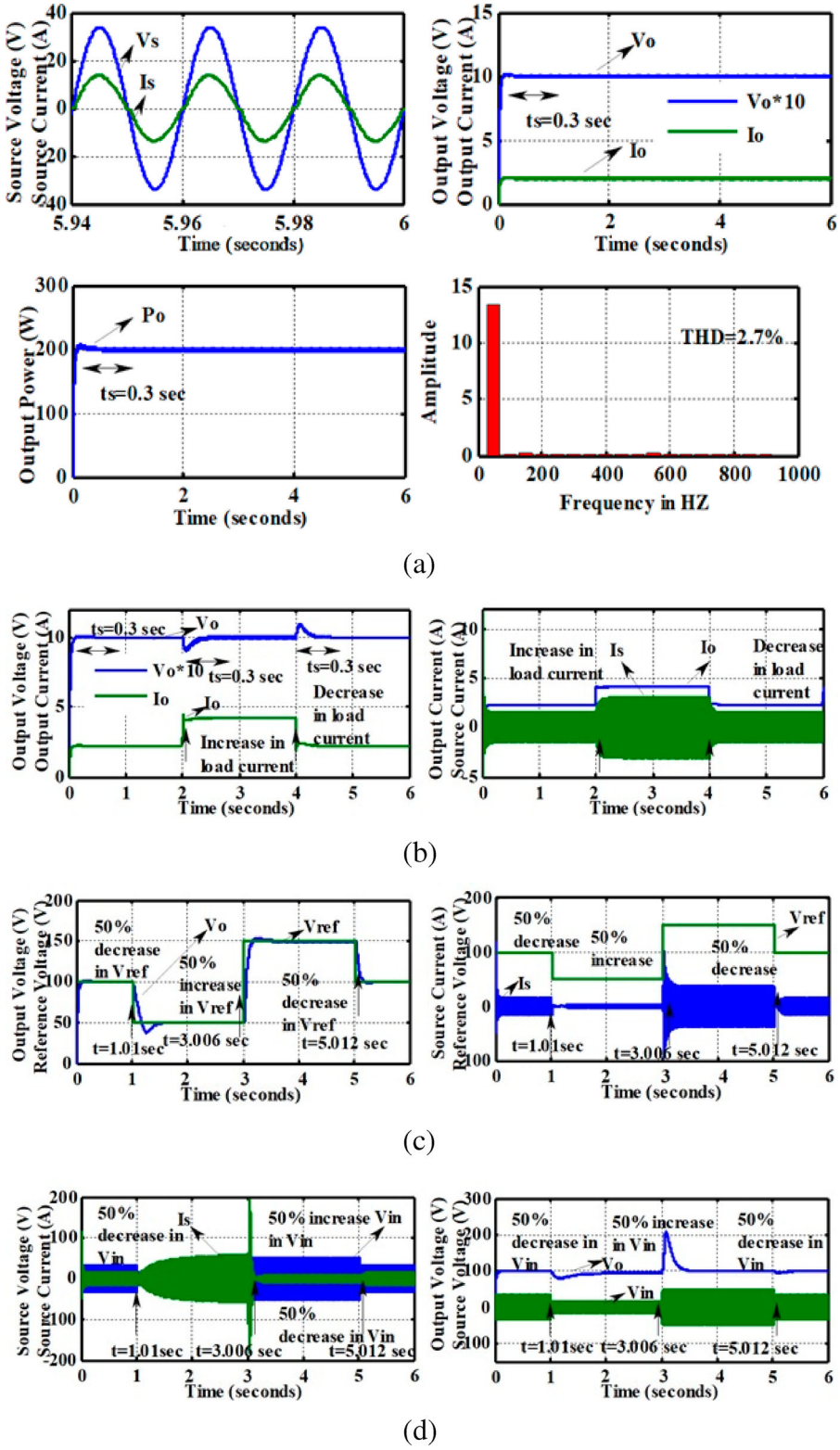

Figure 4. (a) Closed-loop response of the BOCUK PFC converter at rated load; (b): Closed-loop response of the BOCUK PFC converter for load voltage regulation; (c) Closed-loop response of the BOCUK PFC converter for set point variation; (d) Closed-loop response of the proposed converter for line voltage variation.

Table 2. Variation in load resistance of the BOCUK PFC converter.

Load Current (A)	Power Factor	%THD	Settling time (sec)	%Efficiency	%Regulation
2.5	1	3.016	0.162	87.06	−0.1
2.224	1	2.83	0.185	87.47	−0.1
1.924	1	2.62	0.28	87.86	0
1.819	0.99	2.63	0.27	87.96	0
1.667	0.99	2.47	0.23	88.13	0

waveforms of the closed-loop system at the rated load. The results show that the line current tracks the line voltage more closely, resulting in nearly UPF operation. From the harmonic spectrum of line current, % THD is inferred to be 2.7%. Figure 4(b)–(d) depict the simulation results for line, setpoint and load variations.

The line current, load voltage and load current waveforms for increase and decrease in load fluctuations are shown in Figure 4(b). The results illustrate that the load voltage follows the reference voltage after 0.3 s. Figure 4(c) shows the load voltage and load current waveforms for set point variations. At $t = 1.01$ sec, the system is subjected to a 50% drop in V_{ref}, a 50% raise in V_{ref} at $t = 3.012$ s and a 50% drop in V_{ref} at $t = 5.004$ sec. The implemented dual-loop control approach employing LQR- and ASO-tuned PI makes it easier for the load voltage to settle without an undershoot or overshoot. Figure 4(d) depicts the system's response to changes in the line voltage. At $t = 1.01$ s, the system is subjected to a 50% drop in V_{in}, a 50% raise in V_{in} at $t = 3.012$m s and a 50% drop in V_{in} at $t = 5.004$ s. The results show that the LQR controller efficiently tracks the desired load voltage for drop and raise in line voltage.

Table 2 lists numerous performance parameters such as power factor, % THD, settling time, % efficiency and % load regulation. The % efficiency is maintained around 90%, the settling time is between 0.16 s and 0.3 s and the % load regulation is between −0.1 and 0 for fluctuations in load. It is also inferred that the power factor is maintained close to unity and the %THD is below 5% as per IEEE 519-2014 standard, which indicates the robustness of the proposed converter in maintaining the power quality.

5. Experimental results

The proposed dual-loop control employing LQR and ASO-tuned PI controller is realized using a TMS320F28027 digital controller and a laboratory model of the BOCUK PFC converter is constructed for 200 Watts. There are three steps involved in this hardware implementation process: (i) Hall effect voltage and current sensors (LV 25-P, LEM HX 03-P) are employed here to sense the output voltage, rectified voltage and input inductor current and scaling the sensed voltages and currents down to 3.3 V using a signal conditioning circuit. (ii) Realization of the ASO-tuned PI controller to regulate load voltage using the TMS320F28027 processor (iii) Realization of the Inner LQR current controller to shape the line current to follow the line voltage to maintain power factor nearly unity. Figure 5(a) depicts the BOCUK PFC Converter hardware circuit. Figure 5(b) illustrates the hardware implementation of the BOCUK PFC converter. Table 3

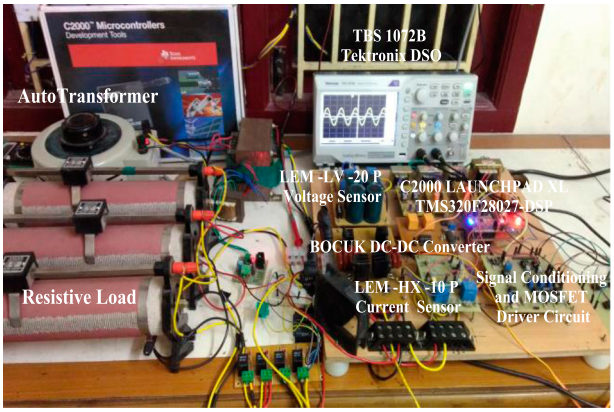

(a)

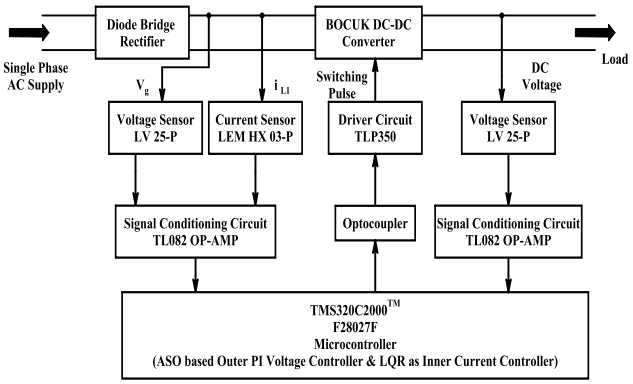

(b)

Figure 5. (a) Experimental prototype model of the BOCUK PFC converter; (b) Hardware implementation of the BOCUK PFC converter.

Table 3. Hardware specification table.

Name of the component	Specifications
Power MOSFET	IRFP250N
Capacitors	2000 µF, 200 V
Diode	MUR 3060
High-frequency inductor	50 kHz, 10 A
Voltage sensor	LV 25-P
Current sensor	LEM HX 03-P
DSP controller	C2000
Transformer for control circuits and Gate driver	12, 6 V, 2 A

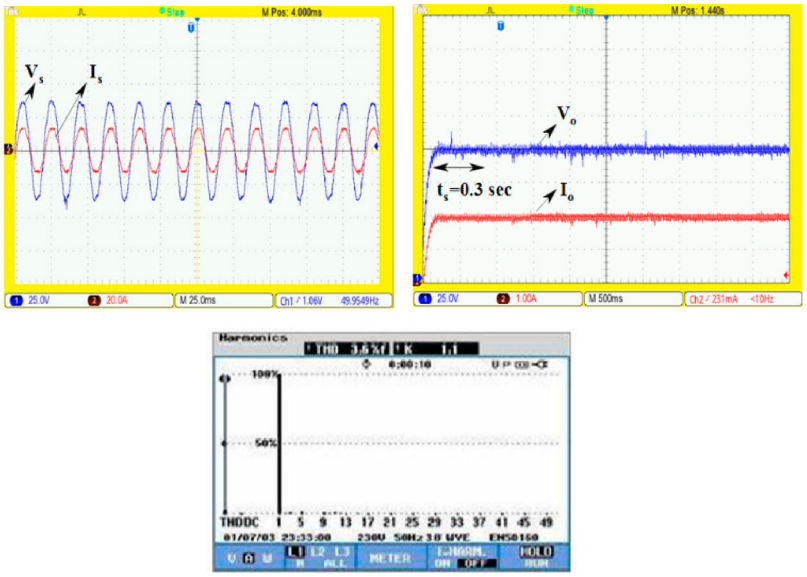

(a)

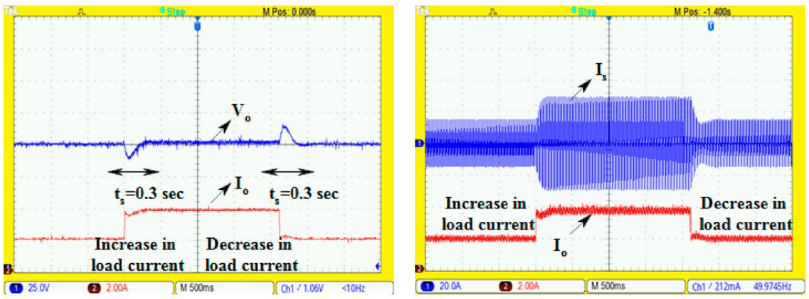

(b)

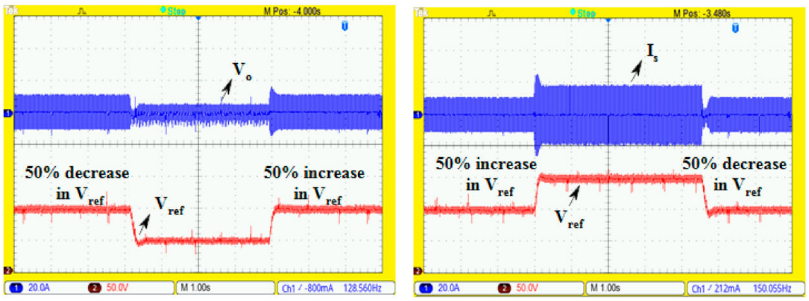

(c)

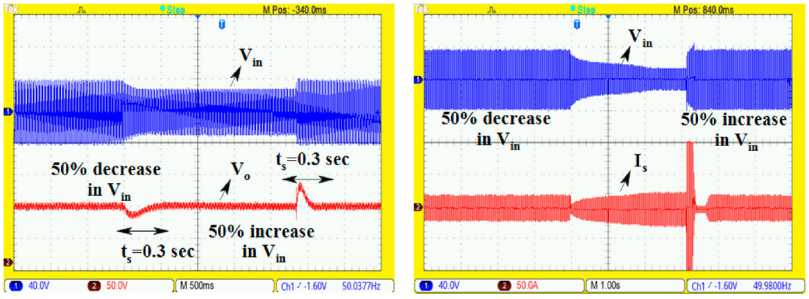

(d)

Figure 6. (a) Closed-loop experimental response of the BOCUK PFC converter for rated load; (b) Closed-loop experimental response of the BOCUK PFC converter for load variations; (c) Closed-loop experimental response of the BOCUK PFC converter for set point variations; (d) Closed-loop experimental response of the BOCUK PFC converter for line variations.

lists the components used and their specifications. The digital controller processes the proposed control algorithms using the sensed Hall effect sensor's voltage and current signals, to compute the new duty ratio to trigger the MOSFET through a TLP350 driver.

Figure 6(a) shows the experimental waveforms for line voltage, line current, load voltage, load current and harmonic spectrum of the line current. The results illustrate that line current follows the line voltage and justifies the UPF operation. THD Spectrum of line current indicates that effective mitigation of line current harmonics makes the % THD as 3.6% as defined by IEEE 519-2014 standard. Figure 6(b)–(d) show the closed-loop experimental response of the BOCUK Converter for variations in load, setpoint and line. From Figure 6(b), it is inferred that load voltage attains the desired value after a settling time of 0.3 s for both raise and drop in load and line current is in phase with the line voltage. Figure 6(c) illustrates that the load voltage tracks the reference voltage effectively. UPF operation and load regulation are also achieved for line variations, as shown in Figure 6(d).

6. Conclusion

The modes of operations of the non-ideal high-gain BOCUK converter operating in CCM were discussed. A mathematical model was obtained using the state-space averaging approach. The second-order model was obtained using Modified HMM. The closed-loop circuit was then constructed and simulated in MATLAB/Simulink software using dual-loop control with an outer ASO-optimized PI and inner LQR current controller. An experimental prototype of the BOCUK PFC converter for 200 Watts was built and implemented with the proposed control algorithms using a TMS320F28027F microcontroller. Simulation and experimental results divulge that the proposed BOCUK converter with dual-loop control using ISE as a fitness function has reduced input current harmonics (2.7% THD) and provides optimal performance with maximum % efficiency (89%) and power factor close to unity. The BOCUK PFC converter with dual-loop control also provides regulated load voltage with minimum settling time for variations in load, line and setpoint making it more appropriate for SMPS applications.

Disclosure statement

No potential conflict of interest was reported by the author(s).

References

[1] Redl R. Power factor correction in single-phase switching-mode power supplies – an overview. Int J Electron. 1994;77(5):555–582.
[2] Gallo CA, Tofoli FL, Correa Pinto JAC. Two-stage isolated switch-mode power supply with high efficiency and high input power factor. IEEE Trans Ind Electron. February 2010;57(11):3754–3766.
[3] Hans MR, Bhagwat NB. Implementation of switched mode power supply with power quality enhancement using zeta converter. International conference on smart electronics and communication (ICOSEC); 2020, 2020. ISBN: 978-1-7281-5461-9 doi:10.1109/icosec49089.2020.9215
[4] Jindong Z, Jovanovic MM, Lee FC. Comparison between CCM single-stage and two-stage boost PFC converters. Proceedings. of IEEE APEC 1999, 1999, pp. 335–341.
[5] Lee JY, Chae HJ. 6.6-kW on-board charger design using DCM PFC converter with harmonic modulation technique and two-stage DC/DC converter. IEEE Trans Ind Electron. 2014;61(3):1243–1252.
[6] Rosseto L, Buso S. Digitally-controlled single-phase single-stage AC/DC PWM converter. IEEE Trans Power Electron 2003;18(1):326–333.
[7] Moschopoulos G, Jain PK. Single-phase single-stage power-factor corrected converter topologies. IEEE Trans Ind Electron. 2005;52(1):23–35.
[8] Lu DDC, Iu HHC, Pjevalica V. A single-stage AC/DC converter with high power factor, regulated bus voltage, and output voltage. IEEE Trans Power Electron 2008;23(1):218–228.
[9] Ma H, Ji Y, Xu Y. Design and analysis of single-stage power factor correction converter with a feedback winding. IEEE Trans Power Electron 2010;25(6):1460–1470.
[10] Cheng H-L, Hsieh Y-C, Lin C-S. Novel single-stage HPF AC/DC converter featuring high circuit efficiency. IEEE Trans Ind Electron. 2012;58:2.
[11] Cho YW, Kwon J-M, Kwon B-H. Single power-conversion AC–DC converter with high power factor and high efficiency. IEEE Trans Power Electron. 2014;29(9):4797–4806.
[12] Durgadevi S, Umamaheswari MG. Analysis and design of single phase power factor correction with DC–DC SEPIC converter for fast dynamic response using genetic algorithm optimized PI controller. IET Circ Devices Syst. 2018;12(2):164–174.
[13] Tibola G, Barbi I. Isolated three-phase high power factor rectifier based on the SEPIC converter operating in discontinuous conduction mode. IEEE Trans Power Electron. 2013;28(11):4962–4969.
[14] Tacca HE. Power factor correction using merged flyback-forward converters. IEEE Trans Power Electron. 2000;15(4):585 –5594.
[15] Luo S, Qiu W, Wu W, et al. Flyboost power factor correction cell and a new family of single-stage AC/DC converters. IEEE Trans Power Electron. 2005;20(1):25–34.
[16] Musavi F, Edington M, Eberle W, et al. Control loop design for a PFC boost converter with ripple steering. IEEE Trans Ind Appl. 2012;49(1):118 –1126.
[17] Umamaheswari MG, Uma G, Vijayalakshmi KM. Analysis and design of reduced-order sliding-mode controller for three-phase power factor correction using Cuk rectifiers. IET Power Electron. May 2013;6(5):935–945.
[18] Umamaheswari MG, Uma G, Annie Isabella L. Analysis and design of digital predictive controller for PFC Cuk converter. J Comput Electron. 2013;13:142–154.
[19] Fernão Pires V, Foito D, Baptista FRB, et al. A photovoltaic generator system with a DC/DC converter based on an integrated Boost-Cuk topology. Sol Energy. 2016;15:1–9.

[20] Marimuthu G, Umamaheswari MG. Analysis and design of single stage bridgeless Cuk converter for current harmonics suppression using particle swarm optimization technique. Electr Power Compon Syst. 2020;47(11–12):1101–1115.
[21] Komathi C, Umamaheswari MG. Design of gray wolf optimizer algorithm-based fractional order PI controller for power factor correction in SMPS applications. IEEE Trans Power Electron. 2020;35(2):2100–2118.
[22] Umamaheswari MG, Uma G, Vijitha R. Comparison of hysteresis control and reduced order linear quadratic regulator control for power factor correction using DC-DC Cuk converters. J Circ Syst Comp. 2012;21(1):1250002.
[23] Umamaheswari MG, Uma G. Analysis and design of reduced order linear quadratic regulator control for three phase power factor correction using Cuk rectifiers. Electr Power Syst Res. 2012;96:1–8.
[24] Palaveashem M, Anbukumar K. Reduced order linear quadratic regulator controller for voltage multiplier cells integrated boost converter. IET Cir Devices Syst. 2016;10(6):536–548.